Monthly Notices
of the
ROYAL ASTRONOMICAL SOCIETY

MNRAS **475,** 2122–2131 (2018)
Advance Access publication 2018 January 9

doi:10.1093/mnras/stx3232

The clustering of galaxies in the completed SDSS-III Baryon Oscillation Spectroscopic Survey: constraining modified gravity

Eva-Maria Mueller,[1]★ Will Percival,[1] Eric Linder,[2,3] Shadab Alam,[4,5,6] Gong-Bo Zhao,[1,7] Ariel G. Sánchez,[8] Florian Beutler[1] and Jon Brinkmann[9]

[1]*Institute of Cosmology and Gravitation, Dennis Sciama Building, University of Portsmouth, Portsmouth PO1 3FX, UK*
[2]*Berkeley Center for Cosmological Physics and Berkeley Lab, University of California, Berkeley, CA 94720, USA*
[3]*Energetic Cosmos Laboratory, Nazarbayev University, Astana 010000, Kazakhstan*
[4]*Department of Physics, Carnegie Mellon University, 5000 Forbes Avenue, Pittsburgh, PA 15213, USA*
[5]*McWilliams Center for Cosmology, Carnegie Mellon University, 5000 Forbes Ave, Pittsburgh, PA 15213, USA*
[6]*Institute for Astronomy, University of Edinburgh, Royal Observatory, Blackford Hill, Edinburgh EH9 3HJ, UK*
[7]*National Astronomy Observatories, Chinese Academy of Science, Beijing 100012, China*
[8]*Max-Planck-Institut für extraterrestrische Physik, Postfach 1312, Giessenbachstr., D-85741 Garching, Germany*
[9]*Apache Point Observatory and New Mexico State University, Sunspot, NM 88349, USA*

Accepted 2017 November 11. Received 2017 October 31; in original form 2016 December 2

ABSTRACT

We use baryon acoustic oscillation and redshift space distortion from the completed Baryon Oscillation Spectroscopic Survey, corresponding to Data Release 12 of the Sloan Digital Sky Survey, combined sample analysis in combination with cosmic microwave background, supernova, and redshift space distortion measurements from additional spectroscopic surveys to test deviations from general relativity. We present constraints on several phenomenological models of modified gravity: First, we parametrize the growth of structure using the growth index γ, finding $\gamma = 0.566 \pm 0.058$ (68 per cent C.L.). Secondly, we modify the relation of the two Newtonian potentials by introducing two additional parameters, $G_{\rm M}$ and $G_{\rm L}$. In this approach, $G_{\rm M}$ refers to modifications of the growth of structure whereas $G_{\rm L}$ to modification of the lensing potential. We consider a power law to model the redshift dependence of $G_{\rm M}$ and $G_{\rm L}$ as well as binning in redshift space, introducing four additional degrees of freedom, $G_{\rm M}(z < 0.5)$, $G_{\rm M}(z > 0.5)$, $G_{\rm L}(z < 0.5)$, and $G_{\rm L}(z > 0.5)$. At 68 per cent C.L., we measure $G_{\rm M} = 0.980 \pm 0.096$ and $G_{\rm L} = 1.082 \pm 0.060$ for a linear model, $G_{\rm M} = 1.01 \pm 0.36$ and $G_{\rm L} = 1.31 \pm 0.19$ for a cubic model as well as $G_{\rm M}(z < 0.5) = 1.26 \pm 0.32$, $G_{\rm M}(z > 0.5) = 0.986 \pm 0.022$, $G_{\rm L}(z < 0.5) = 1.067 \pm 0.058$, and $G_{\rm L}(z > 0.5) = 1.037 \pm 0.029$. Thirdly, we investigate general scalar tensor theories of gravity, finding the model to be mostly unconstrained by current data. Assuming a one-parameter $f(R)$ model, we can constrain $B_0 < 7.7 \times 10^{-5}$ (95 per cent C.L). For all models we considered, we find good agreement with general relativity.

Key words: gravitation – cosmological parameters – dark energy – large-scale structure of Universe – cosmology: observations – cosmology: theory.

1 INTRODUCTION

For the last decade, increasingly accurate cosmological observations, including the latest Planck data sets (Planck Collaboration XIII 2016), have reinforced a simple cosmological model in which general relativity (GR) describes all gravitational interactions, about 70 per cent of the Universe's current energy density is in form of a cosmological constant, and the remaining 30 per cent is dominated by non-relativistic 'dark matter' (e.g. Weinberg et al. 2013). While it is clear that the acceleration mimics the cosmological constant in general effect, the exact physics is unclear, and both new energy-density components and modifications to GR remain possibilities (Copeland, Sami & Tsujikawa 2006; Koyama 2016).

Observational effects of a dynamic energy-density component and modified gravity (MG) are partially degenerate and careful data analysis should take into account both possibilities. However, in general, observations of both cosmological geometry and

★ E-mail: eva-maria.mueller@port.ac.uk

structure growth can distinguish between these options as, in most MG models, the growth of structure is altered compared to GR. Purely geometrical measurements, such as those from supernovae (SNe) and baryon acoustic oscillation (BAO), cannot distinguish between these scenarios (Huterer et al. 2015).

The breakdown of GR opens up a plethora of possible extensions, and no unique physical direction for the modification has yet been favoured. Consequently, recent analyses have focused on generic phenomenological descriptions, dependent on a small number of parameters (Bean & Tangmatitham 2010; Dossett, Ishak & Moldenhauer 2011; Zhao et al. 2012; Asaba et al. 2013; Daniel & Linder 2013; Silvestri, Pogosian & Buniy 2013). These provide a mechanism to test for particular types of behaviour, which, if detected, would provide insight into the type of new physics required. Alternatively, we can think of these phenomenological models as providing complementary tests of GR.

Galaxy redshift surveys provide a number of ways of obtaining cosmological information by exploiting different physical mechanisms that encode information in the observed distribution of galaxies. One of the cleanest measurements is that of the BAO peak, observed within the clustering along (in Δz) and across (in $\Delta\theta$) the line of sight. This large-scale signal is difficult to distort by galaxy formation processes, and allows robust measurements of the Hubble parameter H and the angular diameter distance $D_{\rm A}$ combined with the comoving sound horizon $r_{\rm s}$, which governs the primordial BAO position.

Galaxy surveys also allow measurements of the growth of structure via redshift-space distortions (RSD): the apparent clustering along the line of sight receives a boost when redshifts are translated into distances assuming all of the signal results from the Hubble expansion, with amplitude proportional to the amplitude of correlations in the peculiar velocity field. The amplitude of the additive clustering signal is commonly parametrized by $f(z)\sigma_8(z)$, where $f(z)$ is the growth rate, and $\sigma_8(z)$ is the linear-theory RMS mass fluctuations in spheres of radius $8\,h^{-1}$ Mpc (Song & Percival 2009). Thus, RSD provide a measurement of the rate of growth of cosmological structure, which depends strongly on the large-scale strength of gravity. A review of BAO and RSD measurements is provided in Alam et al. (2017).

In this paper, we use the latest BAO and RSD measurements from the Baryon Oscillation Spectroscopic Survey (BOSS; Dawson et al. 2013), conducted as part of the Sloan Digital Sky Survey III (SDSS-III; Eisenstein et al. 2011), to test for evidence requiring modifications to GR. The data set used is described in Alam et al. (2017), and results from the combination of a number of different measurements of BAO and RSD determined using different methods. In particular, the measurements are a combination of the BAO measurements of Ross et al. (2016) and Beutler et al. (2016) and the fits to the full clustering signal including RSD of Beutler et al. (2017), Sánchez et al. (2017b), Grieb et al. (2017), and Satpathy et al. (2017). These measurements are optimally combined using the method described in Sánchez et al. (2017a), and are provided as correlated measurements of $f\sigma_8$, $D_{\rm A}/r_{\rm s}$, and $Hr_{\rm s}$ at three different redshifts, $z = 0.38$, $z = 0.51$, and $z = 0.61$, which we use along with the 9×9 covariance matrix for these measurements. The RSD measurements are obtained under the assumption of a standard flat Λ cold dark matter (ΛCDM) universe, which could potentially bias the results on more general theories of gravity. Barreira, Sánchez & Schmidt (2016) find, however, that within the context of MG models with scale-independent growth the constraints on $f\sigma_8$ are robust to these assumptions by applying the same analysis pipeline as was used in Sánchez et al. (2017b) and Grieb et al. (2017) to mock catalogues of ΛCDM as well as the normal branch of DGP cosmologies. For models with a scale-dependent growth, a pipeline which fully incorporated the MG model is preferable but beyond the scope of this paper.

Our paper is presented as follows: In Section 2, we discuss the theoretical framework and common parametrizations of MG models. We focus on phenomenological descriptions of MG to connect fundamental theories to observations and to put general constraints on deviations from GR. A summary of the data sets used in this analysis can be found in Section 3. In Section 4, we present the results of performing a Monte Carlo Markov Chain (MCMC) analysis.

2 PARAMETRIZING MODIFICATIONS TO GR

In most theories of MG, the growth of structure is altered from GR; however, there is no unique description of the effect. Therefore, we choose to parametrize deviation from GR in a phenomenological, model-independent way. The following section summarizes the parametrizations considered in this study.

2.1 Growth index

A minimal approach to model deviations from GR is to introduce one additional parameter to the flat ΛCDM model, parametrizing the growth rate through the gravitational growth index γ (Linder 2005; Linder & Cahn 2007) as

$$f(a) = \Omega_{\rm m}(a)^{\gamma} \tag{1}$$

with the scale factor a, $\Omega_{\rm m}(a) = \rho_{\rm m}(a)/[3M_{\rm p}^2H^2(a)]$ where $\rho_{\rm m}$ is the matter background density, $M_{\rm p}$ the Planck mass, and $H(a)$ the Hubble expansion parameter. We also account for the contribution of γ on RMS matter fluctuations today by rescaling σ_8 as

$$\sigma_{8,\gamma}(z) = \sigma_8(0)\frac{D_\gamma(z)}{D_{\rm GR}(0)}\frac{D_{\rm GR}(z_{\rm hi})}{D_\gamma(z_{\rm hi})} \tag{2}$$

with the growth factor calculated as

$$D_\gamma(a) = \exp\left[-\int_a^1 {\rm d}a' f(a')/a'\right] \tag{3}$$

and assuming $z_{\rm hi} = 50$, well in the matter-dominated era.

In GR, we expect the growth index to be approximately constant with $\gamma \approx 0.55$. In this framework, the effect on the background expansion is treated separately from the growth of structure behaviour as an attempt to disentangle dark energy and MG and to investigate the physical nature of extensions to the standard cosmological model. Its simplicity as well as its potential to differentiate between different models makes the growth index parametrization an effective way to test deviations from GR against observations. However, potential scale-dependent behaviour of MG is not captured in this model.

Note that in this parametrization the growth rate is altered directly without modifying the underlying perturbation equations. Thus, only direct growth rate measurements contribute to constraints on γ. The growth index, however, can also be expressed in terms of modifications to the two Newtonian potentials. We will discuss this further in the next section.

2.2 $G_{\rm L}$ and $G_{\rm M}$ parametrization

In the Newtonian gauge, perturbations to the metric can be described by the two gravitational potentials, ϕ and ψ,

$${\rm d}s^2 = a^2[-(1+2\psi){\rm d}\tau^2 + (1-2\phi){\rm d}\boldsymbol{x}^2], \tag{4}$$

where a is the scale factor, τ the conformal time, and $\boldsymbol{x}$ the spatial coordinate. Instead of phenomenologically modelling the growth of structure via the growth index, one can directly alter the evolution of the two gravitational potentials, ϕ and ψ, to account for potential modifications to GR. We can modify the Poisson equations:

$$\nabla^2\psi = 4\pi G a^2 \rho\Delta \times G_{\rm M} \tag{5}$$

$$\nabla^2(\psi+\phi) = 8\pi G a^2 \rho\Delta \times G_{\rm L} \tag{6}$$

introducing the dimensionless parameters $G_{\rm M}$ and $G_{\rm L}$. Here, we have omitted the contribution of the anisotropic stress terms for simplicity since we are mainly interested in modifications to GR that arise in the matter dominated era. The standard GR perturbation equations are recovered for $G_{\rm M} = G_{\rm L} = 1$. $G_{\rm M}$ (short for $G_{\rm matter}$) parametrizes modifications to the growth of structure $\rho\Delta$ through the $\nabla^2\psi$ equation, whereas $G_{\rm L}$ alters the lensing of light, $\nabla^2(\psi+\phi)$. This parametrization of MG has the advantage of allowing direct constraints on the fundamental, linearized perturbation equations as well as connecting to the cosmological observables while minimizing degeneracies between the MG parameters. Note that, in the literature, $G_{\rm M}$ and $G_{\rm L}$ are also referred to as μ and Σ, e.g. see Daniel & Linder (2013), Daniel et al. (2010), Simpson et al. (2013), Zhao et al. (2012), and Song et al. (2011).

Alternatively, one could also use the ratio of the two potentials, referred to as the gravitational slip,

$$\gamma_{\rm slip} = \frac{\phi}{\psi} \tag{7}$$

instead of $G_{\rm L}$ to parametrize the modified Poisson equations.

Measurements of $G_{\rm M}$ and $G_{\rm L}$ can be related back to specific MG theories as well as yielding implications for broad classes of theories. Pogosian & Silvestri (2016) show that, for instance, Horndeski models seem to strongly favour deviations of $G_{\rm M}$ and $G_{\rm L}$ from unity to have the same sign. In general, both MG parameters can be a function of scale and redshift, $G_{\rm M}(k,z)$ and $G_{\rm L}(k,z)$. However, in this paper, we only consider redshift-dependent behaviour, keeping both MG k-independent because of the current lack of a large set of scale-dependent BOSS DR12 RSD measurements (but see Johnson et al. 2014, 2016, and Blake et al. 2016 for other surveys). We model our ignorance of the exact redshift evolution of $G_{\rm M}$ and $G_{\rm L}$ in two ways: First, we assume a simple power-law relation for both parameters

$$G_{\rm X} = 1 + (G_{\rm X}^{(s)} - 1)a^s \tag{8}$$

with $X = \{M, L\}$, considering a constant redshift evolution ($s = 0$), as well as a linear ($s = 1$) and cubic ($s = 3$) model. Here, the superscript (s) in $G_{\rm X}^{(s)}$ indicates the corresponding model.

While these parametrizations are not expected to reflect the actual evolution in many models, they can be viewed as providing a possible indication of deviations from GR. Note however that using a power-law time dependence does not necessarily weight high- and low-redshift data correctly, and could bias the results (Zhao et al. 2012). Therefore, we also consider other parametrizations below. If a signal is seen, then a wide variety of models or more detailed parametrizations should be employed.

Secondly, we bin $G_{\rm M}$ and $G_{\rm L}$ in two redshift bins, $z < 0.5$ and $z > 0.5$, adding four additional parameters to the standard flat ΛCDM model,

$$\boldsymbol{P}_{\rm MG} = \{G_{\rm X}(z<0.5), G_{\rm X}(z>0.5)\} \tag{9}$$

with $X = \{M, L\}$. We limit ourselves to two redshift bins, low-z and high-z, roughly following the DR12 sample split into LOWZ and CMASS.

We modify the publicly available MGCAMB code (Zhao et al. 2009; Hojjati, Pogosian & Zhao 2011), which itself is a modification of the Code for Anisotropies in the Microwave Background (CAMB; Lewis, Challinor & Lasenby 2000), to include these models. We assume that the deviation of GR arises during the matter-dominated era, transitioning from the standard GR perturbation equation to the modified Einstein equation, as given by equations (5) and (6), starting at redshift $z_{\rm MG} < 50$.

In the latter model, however, sharp transitions of $G_{\rm M}$ and $G_{\rm L}$ between the two redshift bins can cause numerical instability which leads to artificial constraints on $G_{\rm L}$ from growth rate observations. We therefore smooth the transition between the bins using an arctan function of width $\Delta z = 0.002$. Note that since MGCAMB evolves the perturbation equation using the μ–$\gamma_{\rm slip}$ parametrization, we apply the smoothing to μ and $\gamma_{\rm slip}$ with $\mu = G_{\rm M}$ and $\gamma_{\rm slip} = 2G_{\rm L}/G_{\rm M} - 1$ in each bin, respectively.

The $G_{\rm M}$–$G_{\rm L}$ formalism can also be related to the growth index γ (see Section 2.1). At subhorizon scales, γ can be expressed in terms of $G_{\rm M}$ following equation 32 of Pogosian et al. (2010):

$$G_{\rm M} = \frac{2}{3}\Omega_{\rm m}^{\gamma-1}\left[\Omega_{\rm m}^{\gamma} + 2 + \frac{H'}{H} + \gamma\frac{\Omega_{\rm m}'}{\Omega_{\rm m}} + \gamma'\ln(\Omega_{\rm m})\right], \tag{10}$$

where primes indicate derivatives with respect to $\ln a$. The $G_{\rm M}$–$G_{\rm L}$ formalism has the advantage of easily including observational constraints from cosmic microwave background (CMB) lensing, weak lensing, or the integrated Sachs–Wolfe (ISW) effect which are ignored when using the implementation outlined in Section 2.1 which only accounts for direct growth rate measurements. Since the growth index only determines $G_{\rm M}$, leaving $G_{\rm L}$ or alternatively the gravitational slip $\phi_{\rm slip}$ undefined, in order to fully apply this formalism, one needs to impose an additional theoretical prior on the model by fixing $G_{\rm L}$ to unity (see e.g. Simpson et al. 2013). Alternatively, one can fix the gravitational slip, $\gamma_{\rm slip} = 1$, as implemented in MGCAMB (Hojjati et al. 2011). Beware that these two approaches are essentially different parametrizations with different underlying theoretical assumptions and different observational effects. Therefore, we will refer to the growth rate parametrization fixing $\gamma_{\rm slip}$ as $\{\gamma\,|\,\text{slip}\}$, and the parametrization fixing $G_{\rm L}$ as $\{\gamma\,|\,G_{\rm L}\}$.

For more details on the relation between the different parametrizations in this framework, see, for instance, Daniel et al. (2010).

2.3 Scalar–tensor theories

Alternatively, to a purely phenomenological description, one can start by considering first principals and a more general form of the Lagrangian to include a wide range of MG models. Using symmetries, self-consistency conditions, and stability requirements, the Lagrangian can be simplified and a general expression for the perturbation equation can be derived.

Here, we consider general scalar–tensor theories using the BZ parametrization (Bertschinger & Zukin 2008; Zhao et al. 2009),

$$G_{\rm M} = \frac{1+\beta_1\lambda_1^2k^2a^s}{1+\lambda_1^2k^2a^s} \tag{11}$$

$$\gamma_{\rm slip} = \frac{1+\beta_2\lambda_2^2k^2a^s}{1+\lambda_2^2k^2a^s} \tag{12}$$

with the gravitational slip, $\gamma_{\rm slip}$, defined as

$$\gamma_{\rm slip} = \frac{\phi}{\psi} \tag{13}$$

and the dimensionless parameters β_1 and β_2 as well as the redshift evolution parameter s and the length-scale parameters λ_1 and λ_2.

This parametrization can capture the effect of most scalar–tensor theories in the quasi-static regime and can be used to test a wide range of MG theories.

A subset of this model can recover $f(R)$ theories: Assuming the relation

$$\beta_1^2 = \frac{\lambda_2^2}{\lambda_1^2} = 2 - \beta_2^2 \frac{\lambda_2^2}{\lambda_1^2} \tag{14}$$

between the length-scale parameters as well setting $\beta_1 = 4/3$ for a fixed coupling between the scalar field and matter, and $s \approx 4$ for viable models (Zhao et al. 2009; Hojjati et al. 2012), leaves us with a one-parameter extension to GR given by

$$B_0 \equiv \frac{2H_0^2\lambda_1^2}{c^2}. \tag{15}$$

3 DATA SETS

In this section, we outline the observational data sets used in our analysis, a combination of large-scale structure (LSS) measurements, CMB experiments as well as supernovae Type Ia (SNe Ia) observations. As with any cosmological constraints resulting from multiple data sets, we have had to choose which data sets to include. Our focus has been on growth of structure measurements, so we have minimized the number of geometrical measurements included in order to reduce the potential for systematic errors. As part of this, we had to decide whether to use the low-redshift distance ladder constraints on H_0 of Riess et al. (2016) as well as higher redshift SN data (Betoule et al. 2014). Either would have demonstrated the effect of improving geometrical constraints. In the end, we chose to use the SN data and no local H_0 measurements given systematic fluctuations in historical low-redshift measurements. However, it is impossible to claim that we did this without knowledge of the well-known $\sim 2\sigma$ tension between Planck and these measurements (Planck Collaboration XIII 2016). Replacing the SN constraints with the low-redshift H_0 measurements would have replicated the 2σ tension in the geometry, without strongly affecting the growth rate. The reader should bear this in mind when interpreting our results.

3.1 BOSS DR12

We use measurements of the post-reconstruction BAO position as a function of direction to the line of sight, and the RSD amplitude, measured from the Data Release 12 (DR12; Alam et al. 2015) of BOSS. These measurements were presented in Alam et al. (2017), and were obtained by optimally combining measurements made using a number of methods including measuring the BAO feature in the correlation function (Ross et al. 2016), and power spectrum (Beutler et al. 2016) multipoles, and RSD from fits to the shape of multipole and angular wedge moments of the correlation function (Sánchez et al. 2017b; Satpathy et al. 2017), and the power spectrum (Beutler et al. 2017; Grieb et al. 2017). The methodology to derive the consensus constraints is discussed in detail in Sánchez et al. (2017a).

The galaxy catalogues used, and mitigation techniques for their nuances are described in detail in Reid et al. (2016), which also presents the targeting algorithm developed to select the galaxies: The galaxies were selected from photometry taken using the Sloan telescope (Gunn et al. 1998, 2006), which was also used for subsequent follow-up spectroscopy (Smee et al. 2013). All the photometry was re-processed and released in the DR8 (Aihara et al. 2011). Details of the spectroscopic data can be found in the DR12 paper (Alam et al. 2015), while the spectroscopic data reduction pipeline and redshift determination are discussed in Bolton et al. (2012).

3.2 CMB

We utilize the temperature C_l^{TT}, low-l polarization C_l^{TE} as well as lensing $C_l^{\phi\phi}$ spectra from the Planck 2015 results (Planck Collaboration XIII 2016). The constraints on MG primarily come from lensing as well as the ISW (Sachs & Wolfe 1967; Kofman & Starobinsky 1985). A more detailed summary about the effects of MG on the CMB can be found in Planck Collaboration XIV (2016).

3.3 SN Ia

We use the joint light-curve analysis (JLA) of SN Ia observations by Betoule et al. (2014), a compilation of 740 SN Ia from the SDSS-II supernovae survey (Frieman et al. 2008; Kessler et al. 2009; Lampeitl et al. 2009; Sollerman et al. 2009; Campbell et al. 2013) as well as the Supernova Legacy Survey (Astier et al. 2006; Sullivan et al. 2011) data. Even though SN Ia observations cannot constrain the growth of structure directly, they provide strong constraints on the cosmological background parameters and hence decrease the overall uncertainty on the expansion history, allowing DR12 to be more effective in looking for any modifications in growth history.

3.4 RSD measurements

In addition to the DR12 BOSS data, we use RSD measurements from three different surveys (see Table 1): the Six-Degree Field Galaxy Survey (6dFGS; Beutler et al. 2012), the SDSS DR7 Main Galaxy Sample (MGS; Howlett et al. 2015), and the VIMOS Public Extragalactic Redshift Survey (VIPERS; de la Torre et al. 2013).

The 6dFGS consists of 81 971 galaxies covering 17 000 deg^2 at low redshifts with $z_{\rm eff} = 0.067$. The growth rate measurement of $f\sigma_8 = 0.423 \pm 0.055$ of Beutler et al. (2012) was obtained modelling the 2D galaxy correlation function. The MGS contains 63 163 galaxies distributed over 6813 deg^2 at $z < 0.2$ yielding to a growth rate of $f\sigma_8 = 0.49^{+0.15}_{-0.14}$, by fitting the two-point correlation function of galaxies in the sample. VIPERS is a high-redshift survey probing the LSS of the universe at $0.5 < z < 1.2$ covering 24 deg^2, measuring the growth rate $f\sigma_8 = 0.47 \pm 0.08$ using the monopole and quadrupole moments of the redshift-space correlations in their analysis. Table 1 summarizes the RSD measurement used in this study.

We do not use the BAO measurements of 6dFGS (Beutler et al. 2011) and MGS since these are likely correlated with the RSD

Table 1. Summary of the growth rate measurements used in this survey in addition to the DR12 BAO + RSD joint analysis.

$f\sigma_8$	$z_{\rm eff}$	Survey	Reference
0.423 ± 0.055	0.067	6dFGS	Beutler et al. (2012)
$0.49^{+0.15}_{-0.14}$	0.15	MGS	Howlett et al. (2015)
0.47 ± 0.08	0.8	VIPERS	de la Torre et al. (2013)

measurement of the corresponding survey. Without a joint analysis of RSD and BAO measurements, or further assessment of the correlation, treating both measurements as independent could potentially lead to biased cosmological constraints. Therefore, we only include the RSD measurements to get the best possible constraints on the growth of structure.

Similarly, due to the slight overlap with BOSS, we do not include the WiggleZ (Blake et al. 2011) and DR7 LRG (Samushia, Percival & Raccanelli 2012) measurements, since both have much less precision than DR12.

4 CONSTRAINTS ON MG

In this section, we perform an MCMC analysis using the publicly available COSMOMC (Lewis & Bridle 2002; Hojjati et al. 2011) with our modifications to the code implemented as discussed in Section 2. We run eight chains for each model until a convergence of $R - 1 < 0.03$ is reached according to the Gelman–Rubin criterion (Gelman & Rubin 1992). We assume a flat ΛCDM background with the MG parameters only affecting the perturbation equations. Therefore, we vary the following cosmological parameters:

$$\boldsymbol{P} = \{w_{\rm cdm}, w_{\rm b}, 100\theta_{\rm MC}, \tau, n_{\rm s}, ln(10^{10}A_{\rm s}), \boldsymbol{X}_{\rm MG}\} \quad (16)$$

with the CDM energy density $w_{\rm cdm} = \Omega_{\rm cdm}h^2$, baryon energy density $w_{\rm b} = \Omega_{\rm b}h^2$, the approximate sound horizon at last scattering $\theta_{\rm MC}$ as used by COSMOMC, reionization optical depth τ, scalar spectral index $n_{\rm s}$, amplitude of the primordial curvature perturbations $A_{\rm s}$, and the MG parameters $X_{\rm MG}$ for a given model. We fix the sum of the neutrino masses to 60 meV and assume an effective number of relativistic species $N_{\rm eff} = 3.046$.

4.1 Growth index

Fig. 1 shows the DR12 BAO + RSD consensus constraints in combination with other data sets (see Section 3) in the σ_8–γ plane, adding the growth index γ as a one-parameter, MG extension to the base flat ΛCDM. Here, we use the γ parametrization as outlined in Section 2.1, directly altering the growth rate as well as the RMS matter fluctuations, without relating γ to the fundamental perturbation equation. The constraints on γ consequently derive from the RSD measurements, while the other data sets only constrain the cosmological background. None the less, we are including these data sets to maintain consistency among the different parametrization considered in this paper.

We find excellent agreement with GR measuring $\gamma = 0.558 \pm 0.086$ at 68 per cent C.L. from the DR12 consensus measurements including Planck temperature compared to the six-parameter base flat ΛCDM model. The improvement of the fit when varying γ is marginal with $\Delta\chi^2 = 0.1$ compared to ΛCDM, albeit with higher complexity of the model. The constraints tighten when adding in further data sets yielding to a 10 per cent measurement uncertainty on the MG parameter, $\gamma = 0.566 \pm 0.058$, from DR12 BAO + RSD, CMB, SN, and other RSD measurements.

Our results are in good agreement with Sánchez et al. (2017b), who found $\gamma = 0.609 \pm 0.079$ combining BOSS DR12 configuration space wedges measurements with Planck data as well as with Grieb et al. (2017), who quote $\gamma = 0.52 \pm 0.10$ using Fourier wedges. $\gamma = 0.52 \pm 0.10$ using Fourier space wedges. We can improve upon previous studies, i.e. Beutler et al. (2014), by 30–40 per cent.

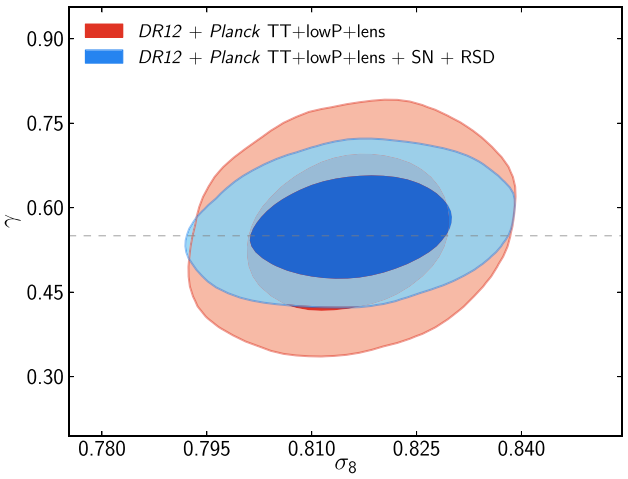

Figure 1. 68 per cent and 95 per cent constraints on the MG parameter γ and σ_8 in the base γΛCDM model, using the DR12 BAO+RSD combined analysis and Planck temperature, low-ℓ polarization, and lensing (red contours), and including RSD measurement from additional LSS surveys as well as SN data as described in Section 3 (blue contours). Here, we use the γ parametrization as described in Section 2.1, modifying directly the growth rate and RMS matter fluctuations. Thus, the constraints on γ purely come from the RSD measurements with the other data sets only constraining the background parameters. The dashed line shows the GR prediction for the growth index, $\gamma \approx 6/11$ (Linder 2005).

As outlined in Section 2, there is a subtlety in how the γ formalism is applied when relating γ to the Newtonian potentials to include effects of CMB lensing, weak lensing or the ISW effect. Instead of just parametrizing the growth of structure (see Section 2.1), one can approximate the Newtonian potential ψ in terms of γ and evolve the modified perturbation equation as implemented in MGCAMB, fixing either the ratio of the two potentials to unity, $\gamma_{\rm slip} = 1$, or fixing $G_{\rm L} = 1$; we denoted the former as the $\{\gamma \,|\, {\rm slip}\}$ formalism and the latter $\{\gamma \,|\, G_{\rm L}\}$. We measure $\gamma = 0.513 \pm 0.027$ at 68 per cent C.L. in the $\{\gamma \,|\, {\rm slip}\}$ parametrization including effects of CMB lensing and the ISW effect. Using the $\{\gamma \,|\, G_{\rm L}\}$ formalism, we find $\gamma = 0.529 \pm 0.067$ at 68 per cent C.L. We find differences in the observational constraints because of the underlying theoretical assumption since the $\{\gamma \,|\, G_{\rm L}\}$ implementation leaves the gravitational lensing potential unchanged. Our measurement when including effects of CMB lensing, weak lensing or the ISW effect of the growth index is in good agreement with previous studies. For instance, Alam, Ho & Silvestri (2016) found $\gamma = 0.477 \pm 0.096$ at 68 per cent C.L. for $\{\gamma \,|\, {\rm slip}\}$ using CMASS DR11 and Planck 2013 angular power spectrum data and $\gamma = 0.612 \pm 0.072$ using data from the *Planck* satellite in combination with six LSS surveys; Johnson et al. (2016) quote $\gamma = 0.665 \pm 0.0669$ at 68 per cent C.L. using the $\{\gamma \,|\, G_{\rm L}\}$ parametrization for a combination of multipole measurements from WiggleZ and BOSS, velocity power measurements from the 6dF survey as well as additional BAO, SN, CMB, and ISW measurements.

4.2 $G_{\rm M}$–$G_{\rm L}$ parametrization

Fig. 2 shows the 68 per cent and 95 per cent confidence regions of $G_{\rm M}$ and $G_{\rm L}$ assuming a constant model ($s = 0$) for different data sets. Here, we have fixed the other cosmological parameters to highlight the degeneracy between the MG parameters of the

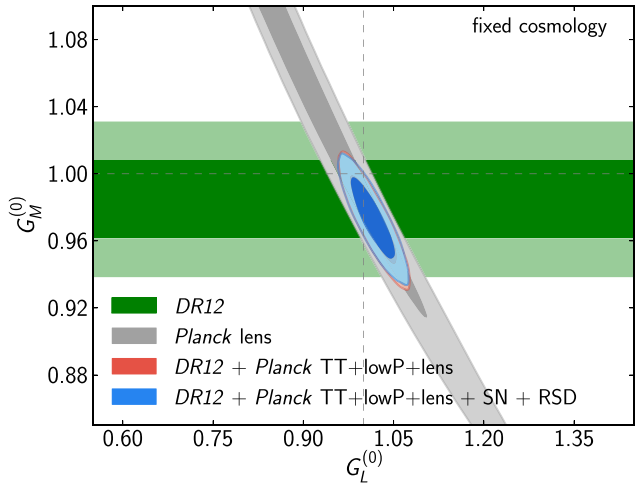

Figure 2. Joint 68 per cent (dark shaded) and 95 per cent (light shaded) C.L. for the MG parameters $G_{\rm M}^{(0)}$ and $G_{\rm L}^{(0)}$ assuming a constant model, as defined in Section 2.2, and fixing all other cosmological parameters to their Planck best-fitting value to highlight the degeneracies between the two MG parameters; this figure should not be viewed as giving cosmological confidence regions. We consider the following data sets: DR12 (green contours), Planck lensing (grey contours), DR12 + Planck temperature, low-ℓ polarization and lensing (red contours), and DR12 + Planck temperature, low-ℓ polarization and lensing + SN + RSD (blue contours) (for details on the data sets, see Section 3). $G_{\rm M}$ is mainly constrained by LSS RSD measurements whereas the uncertainty on $G_{\rm L}$ is given by lensing measurements.

different cosmological probes. The DR12 combined sample BAO and RSD measurement can constrain $G_{\rm M}$, whereas the uncertainty on $G_{\rm L}$ is determined by CMB lensing in accordance to their definition (see Section 2.2). The combination of both growth of structure and lensing measurements yields tight constraints on MG. The results of our MCMC analysis now marginalizing over the flat ΛCDM cosmological parameters are displayed in Fig. 3 and summarized in Table 2. Note that the 95 per cent C.L. tension with GR seen in Fig. 2 with fixed cosmology goes away when fully marginalizing over all cosmological parameters. We find excellent agreement

Table 2. Summary of the 68 per cent C.L. constraints on $G_{\rm M}$ and $G_{\rm L}$, marginalized over the ΛCDM parameters, from the MCMC analysis for a constant, linear, and cubic model corresponding to the blue contours of Fig. 3.

Model	$G_{\rm M}^{(s)}$	$G_{\rm L}^{(s)}$
$s = 0$: constant	0.991 ± 0.022	1.030 ± 0.030
$s = 1$: linear	0.980 ± 0.096	1.082 ± 0.060
$s = 3$: cubic	1.01 ± 0.36	1.31 ± 0.19

with GR for all models and data sets considered, finding both parameters to be unity within 1σ. The errors increase with a stronger redshift dependence since deviations from GR have a smaller impact at high redshift, i.e. $G_{\rm X}^{(s)}$ contributes less to the overall $G_{\rm X}$ defined as $G_{\rm X} = 1 + (G_{\rm X}^{(s)} - 1)a^s$. Therefore, the constant model is the best constrained with the smallest uncertainty and the cubic model the least constrained with large errors. Note how assuming a particular redshift dependence can shift the contours. Including additional RSD measurements in the DR12 data set can improve the constraints, in particular for the cubic model, since additional measurements constrain the growth of structure over a larger redshift range. The χ^2 for all three models is comparable, showing no preference for a particular redshift evolution, with $\Delta\chi^2 < 0.1$ compared to ΛCDM.

Secondly, we consider a model with the MG parameters binned in redshift space. Fig. 4 displays the constraints on $G_{\rm M}(z)$ and $G_{\rm L}(z)$ for two redshifts, $z < 0.5$ and $z > 0.5$, extending the standard ΛCDM model by a total of four extra parameters. The red contours show the uncertainty derived from the DR12 in combination with Planck temperature (TT), low-ℓ polarization (lowP), and lensing data whereas the blue contours include additional SN and RSD measurements as described in Section 3.3 and Section 3.4. The errors on $G_{\rm M}(z)$ are improved significantly by adding in additional growth rate measurements at multiple redshifts since $G_{\rm M}$ alters the growth of structure. The improvements on $G_{\rm L}$, however, are smaller because the constraints on $G_{\rm L}(z)$ are dominated by CMB lensing and the ISW effect. Using all data sets, the 68 per cent C.L. results

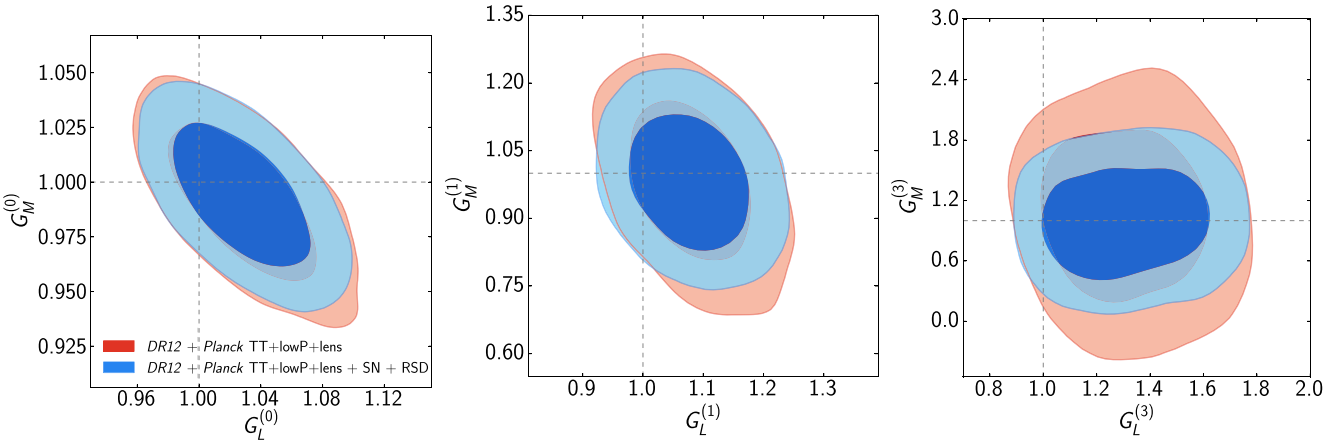

Figure 3. 68 per cent and 95 per cent confidence region of the MG parameters $G_{\rm M}$ and $G_{\rm L}$ parametrized as $G_{\rm X} = 1 + (G_{\rm X}^{(s)} - 1)a^s$, assuming a constant redshift evolution with $s = 0$ (left-hand panel), linear with $s = 1$ (middle panel), and cubic with $s = 3$ (right-hand panel). Note the very different scales. A stronger redshift dependence loosens up the constraints since the effect of MG is diminished at high redshift, leaving the cubic model to be the least constrained scenario. In the constant model, however, deviations from GR start growing at high redshifts yielding tight constraints. The dashed grey lines show the GR prediction of the MG parameters $G_{\rm M} = G_{\rm L} = 1$.

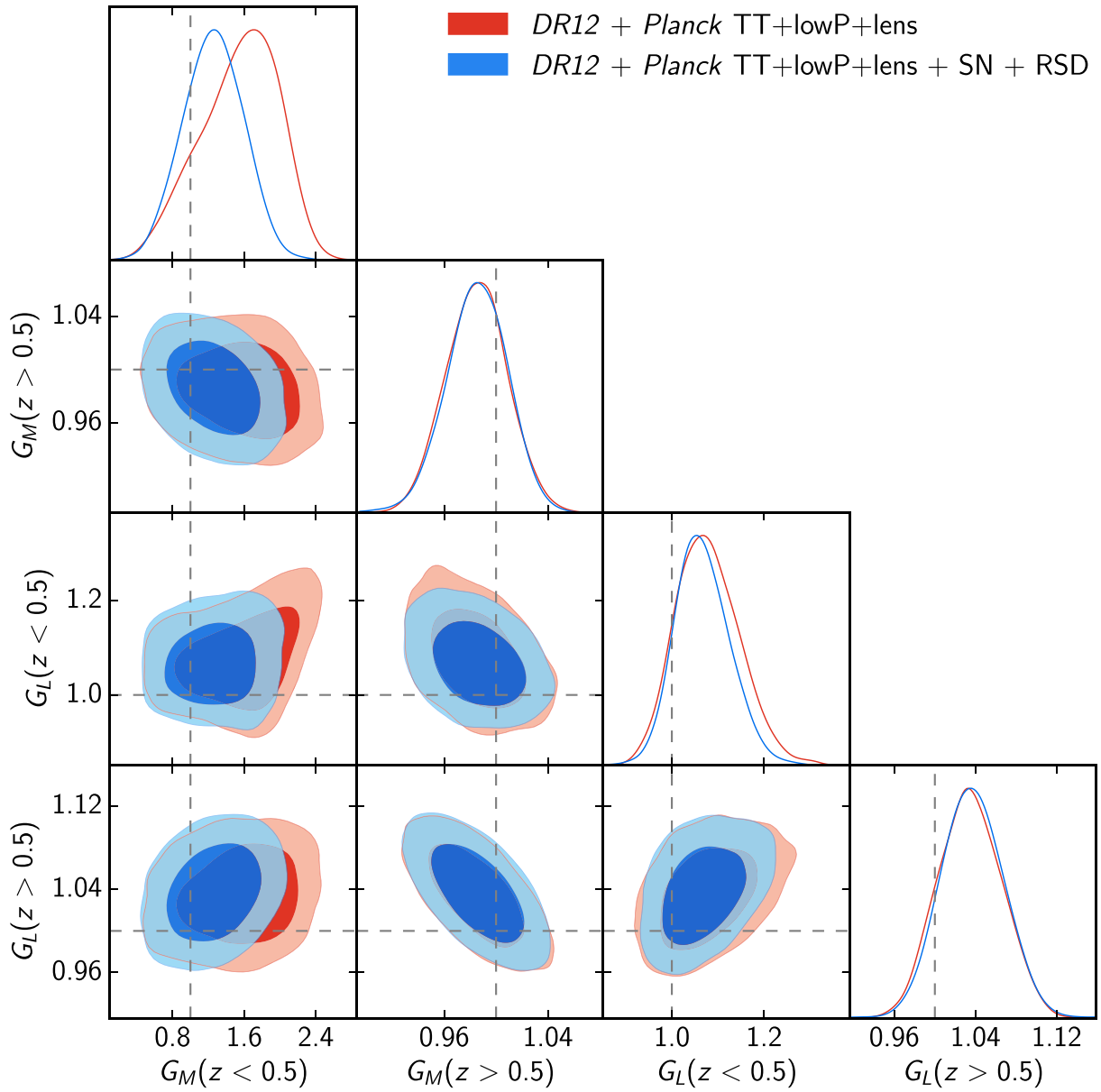

Figure 4. 68 per cent (dark shaded) and 95 per cent (light shaded) C.L. on the MG parameters G_M–G_L considering two redshift bins, $z < 0.5$ and $z > 0.5$ for different data sets: DR12 + Planck (red contours) and DR12+Planck+SN+RSD (blue contours). Including further LSS measurements in the DR12 sample can significantly improve the constraints on G_M as the growth of structure is measured over a larger redshift range, especially to lower redshifts. However, the uncertainty on G_L is dominated by CMB lensing and ISW measurements and therefore does not improve upon including additional RSD measurements. Dashed grey lines show the GR prediction, $G_M = G_L = 1$.

are

$$
\begin{aligned}
G_M(z < 0.5) &= 1.26 \pm 0.32, \\
G_M(z > 0.5) &= 0.986 \pm 0.022, \\
G_L(z < 0.5) &= 1.067^{+0.050}_{-0.064}, \\
G_L(z > 0.5) &= 1.037 \pm 0.029,
\end{aligned}
\tag{17}
$$

in very good agreement with GR at the 68 per cent C.L. We find no significant improvement of the fit to the data compared to ΛCDM with $\Delta\chi^2 = 0.25$.

Our results are consistent with previous studies with slight differences arising due to the usage of different data sets: Johnson et al. (2016) derive constraints on G_M and G_L, binned in both redshift and scale, using multiple measurements from the WiggleZ and BOSS DR11 CMASS and velocity power measurements from the 6dF survey in combination with CMB and SN data, confirming GR at 95 per cent C.L. Song et al. (2011) adopt a linear and cubic model for G_M and G_L with a combination of peculiar velocity and weak lensing measurements finding consistency with GR. For further studies, see for instance Daniel et al. (2010), Simpson et al. (2013), and Planck Collaboration XIV (2016).

4.3 Scalar–tensor theories

Fig. 5 shows the likelihood constraints on the parameters of the BZ model, including a prior on s given in Table 3. As s tends to infinity, we see from equation (12) that the terms that depend on β_1 and β_2 become negligible, except at very low redshifts. Consequently, in

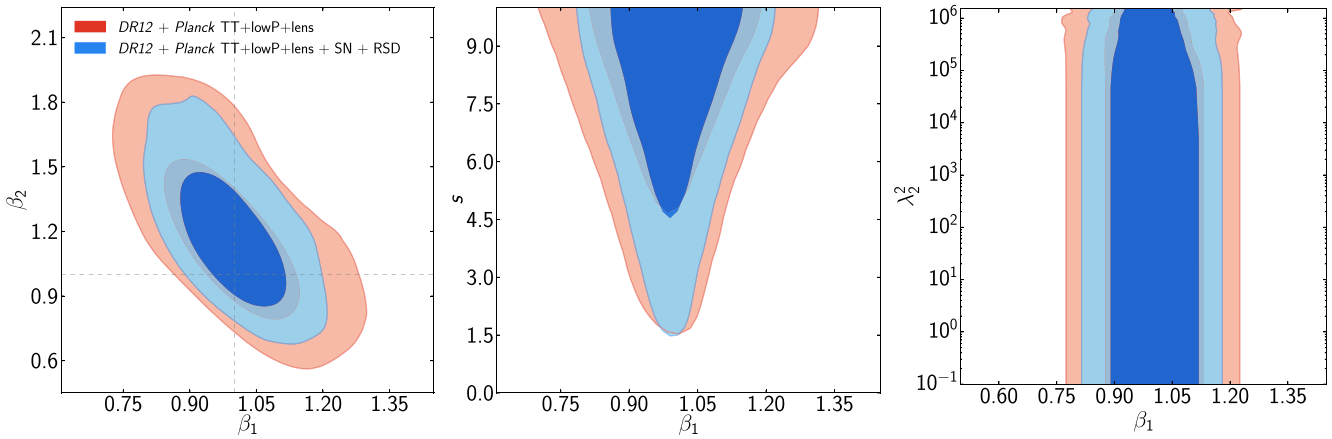

Figure 5. 2D contours of the BZ parameters, β_1–β_2 (left-hand panel), β_1–s (middle panel), and β_1–λ_2^2 (right-hand panel) for the DR12 combined analysis + Planck measurements (red contours) as well as including SNe data and further RSD measurements as discussed in Section 3 (blue contours). The constraints run into the upper limit of the prior on s; larger s would allow more extreme values of the other parameters, while smaller s would tighten the constraints (also see Fig. 6).

Table 3. Summary of the priors on the scalar–tensor theory parametrization. All priors are linear.

Model	Parameter	Prior range
BZ	β_1	0–3
	β_2	0–3
	λ_1^2	(0–2) $\times$ 10^6 Mpc^2
	λ_2^2	(0–2) $\times$ 10^6 Mpc^2
	s	0–10
$f(R)$	B_0	0–0.01

this limit, β_1 and β_2 can take any value without changing the model. If the data allow this limit, then we see that the β_1 and β_2 constraints are degenerate with the upper limit placed on s by the prior. In effect, we would only find meaningful constraints on β_1 and β_2 if we also measure s. Fig. 5 shows that this is not the case for the data sets under consideration, and consequently, the constraints on β_1 and β_2 shown in the left-hand panel of Fig. 5 are purely determined by the upper limit of the prior on s. Consequently, we do not quote any parameter measurements for this model. The constraints on β_1 and β_2 for different priors on s can be found in Fig. 6. Decreasing the prior range on s reduces the uncertainty on β_1 and β_2 significantly.

Fig. 7 shows the constraints on B_0 in the one-parameter $f(R)$ model as defined in Section 2.3. We find an upper limit of $B_0 < 7.7 \times 10^{-5}$ at 95 per cent C.L. including all data sets considered in this study. Neither model is favoured by the data compared to ΛCDM in our analysis. Note that we applied a linear prior on B_0 to sample its distribution function. Alternatively, one could assume a logarithmic prior on B_0 instead, to give equal weight to large and small scales. The caveat of this approach, however, is that the range of $\log B_0$ is unknown a priori, introducing a dependence of the constraints on the lower limit of the prior. Since for all values of $\log B_0 < -6$, $f(R)$ mimics ΛCDM, we adopt a prior on $\log B_0$ of $[-6,-2]$, as in Song et al. (2015). We find an upper limit of $\log B_0 < -4.54$ at 95 per cent C.L.

Another caveat in our analysis is that the BZ as well as $f(R)$ parametrization is k-dependent whereas all RSD observations measure $f\sigma_8(z)$ at an effective scale of $k \approx 0.15$–$0.2\,h\,\mathrm{Mpc}^{-1}$. Calculating $f\sigma_8(z)$ averaged over all scales as implemented in COSMOMC could potentially bias the results. Alam et al. (2016) find that using

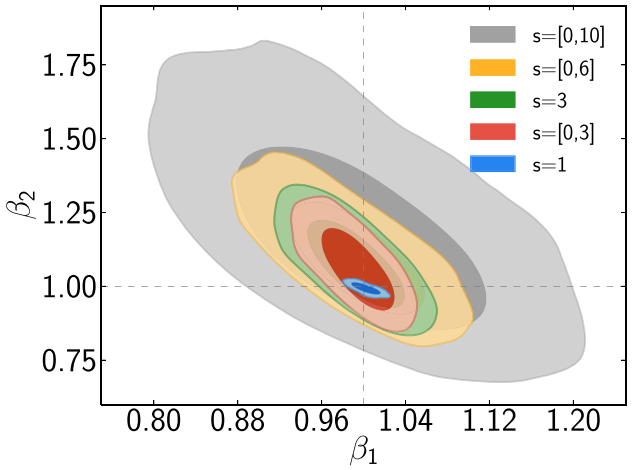

Figure 6. 2D contours of the BZ parameters, β_1–β_2, for different assumptions on s using DR12+Planck+SN+RSD data; grey contours assuming a prior range for s of $s = [0, 10]$, orange contours refer to $s = [0, 6]$, red to $s = [0, 3]$ while the green contours are for a model with s fixed to 3, and blue for $s = 1$.

the growth rate calculated at $k = 0.2\,h\,\mathrm{Mpc}^{-1}$ instead of averaged over k reduced the error on B_0 by 30–40 per cent. In general, an RSD measurement binned in redshift as well as scale $f(z, k)$ would be necessary to improve upon the errors on the BZ parameters and to detect a scale-dependent deviation from gravity. We leave this analysis for future work.

5 CONCLUSIONS

In this paper, we have used recent galaxy clustering measurements made from the BOSS DR12 data to test for evidence supporting models that modify gravity beyond GR. We consider a number of extensions to the flat ΛCDM+GR model inspired by modifications to GR, and test whether these extensions are supported by the data. One of the simplest such model is the γ parametrization of the growth rate, which we introduced in Section 2.1. In fact, we highlighted a subtlety in the common implementation of this model, in that people often express γ in terms of the Newtonian potentials

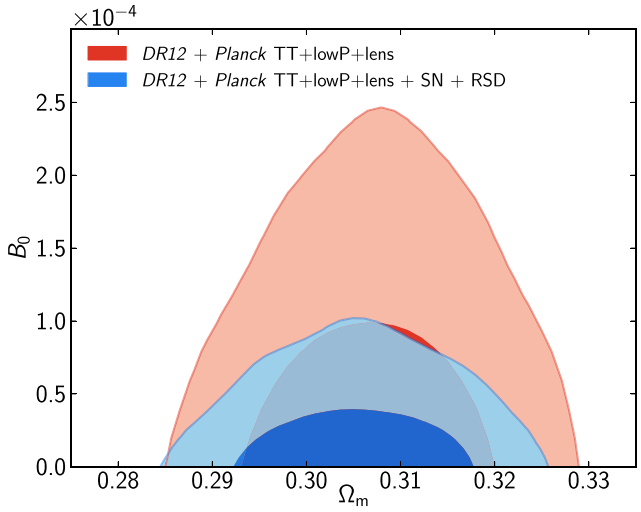

Figure 7. 2D contours of the $f(R)$ parameter B_0. The red contours refer to the DR12 combined analysis + Planck measurements ($B_0 < 2.0 \times 10^{-4}$ at 95 per cent C.L.), whereas the blue contours include SN as well as additional RSD measurements ($B_0 < 7.7 \times 10^{-5}$ at 95 per cent C.L.).

in order to combine γ with additional observations, and we highlight two of these, which we call $\{\gamma \,|\, \mathrm{slip}\}$ and $\{\gamma \,|\, G_\mathrm{L}\}$, and we compare constraints from all three in Section 4.1. When comparing measurements made in different analyses, or in implementations in packages such as MGCAMB, which uses the $\{\gamma \,|\, \mathrm{slip}\}$ assumption, it is important to understand which model is being used. Moving beyond γ, we have introduced, in Section 2.2, dimensionless parameters G_M and G_L into the Einstein equations allowing non-GR evolution of the gravitational potentials ϕ and ψ. Finally, we consider a five-parameter BZ parametrization of deviations from GR as well as a one-parameter $f(R)$ model, introduced in Section 2.3.

The BOSS DR12 measurements, along with those from the CMB, are considered the most robust as they rely on simple physical processes and minimal additional modelling. The comparison between BOSS BAO and RSD measurements compares expansion and structure growth, which is particularly powerful for making such measurements and testing GR, and the BOSS DR12 measurements are the most accurate to date. To extend the redshift range covered, we combine the BOSS measurements with BAO and RSD from the 6dFGS, VIPERS, and the SDSS MGS, chosen because they do not spatially overlap with BOSS. As well as the LSS data, we include Planck CMB measurements, excluding polarization data because of potential calibration issues, and the JLA SNe data to better constrain the expansion history, allowing DR12 to better explore the growth history. These data sets were introduced in Section 3.

Results from the fits to data are presented in Section 4. For the γ parametrization, we see significant changes in the confidence intervals depending on the exact implementation: γ, $\{\gamma \,|\, \mathrm{slip}\}$ or $\{\gamma \,|\, G_\mathrm{L}\}$, but all are consistent with GR. For the parametrizations with more free parameters, we again see that the ΛCDM+GR model is an acceptable fit, showing no evidence requiring MG.

Even though we have found no evidence requiring modifications to GR in the data sets analysed, there are a number of observations in mild tension with the simple ΛCDM+GR cosmological model. Given the free parameters within the ΛCDM+GR framework, these tensions generally show up when ΛCDM parameter measurements, made using different data, are compared. One source of tension is shown when the lensing measurements of the amplitude of matter clustering from CFHTLS (Heymans et al. 2012) and KiDS (Hildebrandt et al. 2017) are compared to those made with Planck CMB measurements including CMB lensing, with the KiDS data showing a 2.3σ tension with the Planck 2015 results (Hildebrandt et al. 2017). There are also data sets where there is a mild tension between measurements using the same probes: e.g. between the Planck 2015 results and those from combining *WMAP*, SPT, and ACT (Calabrese et al. 2013; Hinshaw et al. 2013; Sievers et al. 2013; Story et al. 2013). In addition, several high-precision direct measurements of H_0 measure values about 10 per cent higher than those inferred from combinations of *Planck* and BOSS BAO data (Riess et al. 2011, 2016; Freedman et al. 2012; Alam et al. 2017). The DR12 analysis of Gil-Marín et al. (2017) presents a 2.5σ tension with the ΛCDM+GR model driven by measurements of the redshift-space bispectrum. While this level of tension is potentially interesting, it relies on modelling the redshift-space bispectrum, a less established field compared with modelling BAO and RSD measurements. In our analysis, we have included measurements from two-point clustering only, finding good consistency with the flat ΛCDM+GR model. None of these 'discrepancies' is at the level of providing strong evidence for a breakdown of the simple ΛCDM+GR model, and underestimated systematic and/or statistical errors in one of more measurements cannot be ruled out at this stage.

The recently reported tension of $f\sigma_8$ measurements from RSD measurements being lower than ΛCDM+GR expectations (Macaulay, Wehus & Eriksen 2013) has been alleviated by the recent BOSS DR12 results, which are within 1σ of the expectation (Alam et al. 2017). Our work using these data and other to look for evidence of modified GR further supports the view that there is no remaining tension in the RSD measurements.

ACKNOWLEDGEMENTS

EM would like to thank Rachel Bean and Levon Pogosian for helpful discussions. EM and WJP acknowledge support from the European Research Council through the Darksurvey Grant 614030. WJP also acknowledges support from the UK Science and Technology Facilities Council Grant ST/N000668/1 and the UK Space Agency Grant ST/N00180X/1. EL thanks the Aspen Center for Physics, which is supported by NSF Grant PHY-1066293, for a motivating environment. This work is supported in part by the Energetic Cosmos Laboratory and by the US Department of Energy, Office of Science, Office of High Energy Physics, under Award DE-SC-0007867 and contract no. DE-AC02-05CH11231. AGS acknowledges support from the Trans-regional Collaborative Research Centre TR33 'The Dark Universe' of the German Research Foundation (DFG). FB acknowledges support from the UK Space Agency through Grant ST/N00180X/1. GBZ is supported by the NSFC Grant No. 11673025, by the Strategic Priority Research Program 'The Emergence of Cosmological Structures' of the Chinese Academy of Sciences Grant No. XDB09000000, and by University of Portsmouth. SA is supported by the European Research Council through the COSFORM Research Grant (#670193).

Funding for SDSS-III has been provided by the Alfred P. Sloan Foundation, the Participating Institutions, the National Science Foundation, and the U.S. Department of Energy Office of Science. The SDSS-III web site is http://www.sdss3.org/.

SDSS-III is managed by the Astrophysical Research Consortium for the Participating Institutions of the SDSS-III Collaboration including the University of Arizona, the Brazilian Participation Group, Brookhaven National Laboratory, Carnegie Mellon University, University of Florida, the French Participation Group, the

German Participation Group, Harvard University, the Instituto de Astrofisica de Canarias, the Michigan State/Notre Dame/JINA Participation Group, Johns Hopkins University, Lawrence Berkeley National Laboratory, Max Planck Institute for Astrophysics, Max Planck Institute for Extraterrestrial Physics, New Mexico State University, New York University, Ohio State University, Pennsylvania State University, University of Portsmouth, Princeton University, the Spanish Participation Group, University of Tokyo, University of Utah, Vanderbilt University, University of Virginia, University of Washington, and Yale University.

REFERENCES

Aihara H. et al., 2011, ApJS, 193, 29
Alam S. et al., 2015, ApJS, 219, 12
Alam S., Ho S., Silvestri A., 2016, MNRAS, 456, 3743
Alam S. et al., 2017, MNRAS, 470, 2617
Asaba S., Hikage C., Koyama K., Zhao G.-B., Hojjati A., Pogosian L., 2013, J. Cosmol. Astropart. Phys., 1308, 029
Astier P. et al., 2006, A&A, 447, 31
Barreira A., Sánchez A. G., Schmidt F., 2016, Phys. Rev. D, 94, 084022
Bean R., Tangmatitham M., 2010, Phys. Rev. D, 81, 083534
Bertschinger E., Zukin P., 2008, Phys. Rev. D, 78, 024015
Betoule M. et al., 2014, A&A, 568, A22
Beutler F. et al., 2011, MNRAS, 416, 3017
Beutler F. et al., 2012, MNRAS, 423, 3430
Beutler F. et al., 2014, MNRAS, 443, 1065
Beutler F. et al., 2016, MNRAS, 464, 3409
Beutler F. et al., 2017, MNRAS, 466, 2242
Blake C. et al., 2011, MNRAS, 415, 2876
Blake C. et al., 2016, MNRAS, 456, 2806
Bolton A. S. et al., 2012, AJ, 144, 144
Calabrese E. et al., 2013, Phys. Rev. D, 87, 103012
Campbell H. et al., 2013, ApJ, 763, 88
Copeland E. J., Sami M., Tsujikawa S., 2006, Int. J. Mod. Phys., D15, 1753
Daniel S. F., Linder E. V., 2013, J. Cosmol. Astropart. Phys., 1302, 007
Daniel S. F., Linder E. V., Smith T. L., Caldwell R. R., Cooray A., Leauthaud A., Lombriser L., 2010, Phys. Rev. D, 81, 123508
Dawson K. S. et al., 2013, AJ, 145, 10
de la Torre S. et al., 2013, A&A, 557, A54
Dossett J. N., Ishak M., Moldenhauer J., 2011, Phys. Rev. D, 84, 123001
Eisenstein D. J. et al., 2011, AJ, 142, 72
Freedman W. L., Madore B. F., Scowcroft V., Burns C., Monson A., Persson S. E., Seibert M., Rigby J., 2012, ApJ, 758, 24
Frieman J. A. et al., 2008, AJ, 135, 338
Gelman A., Rubin D. B., 1992, Stat. Sci., 7, 457
Gil-Marín H., Percival W. J., Verde L., Brownstein J. R., Chuang C.-H., Kitaura F.-S., Rodríguez-Torres S. A., Olmstead M. D., 2017, MNRAS, 465, 1757
Grieb J. N. et al., 2017, MNRAS, 467, 2085
Gunn J. E. et al., 1998, AJ, 116, 3040
Gunn J. E. et al., 2006, AJ, 131, 2332
Heymans C. et al., 2012, MNRAS, 427, 146
Hildebrandt H. et al., 2017, MNRAS, 465, 1454
Hinshaw G. et al., 2013, ApJS, 208, 19
Hojjati A., Pogosian L., Zhao G.-B., 2011, J. Cosmol. Astropart. Phys., 1108, 005
Hojjati A., Pogosian L., Silvestri A., Talbot S., 2012, Phys. Rev. D, 86, 123503
Howlett C., Ross A., Samushia L., Percival W., Manera M., 2015, MNRAS, 449, 848
Huterer D. et al., 2015, Astropart. Phys., 63, 23
Johnson A. et al., 2014, MNRAS, 444, 3926
Johnson A., Blake C., Dossett J., Koda J., Parkinson D., Joudaki S., 2016, MNRAS, 458, 2725
Kessler R. et al., 2009, ApJS, 185, 32
Kofman L., Starobinsky A. A., 1985, Sov. Astron. Lett., 11, 271
Koyama K., 2016, Rep. Prog. Phys., 79, 046902
Lampeitl H. et al., 2009, MNRAS, 401, 2331
Lewis A., Bridle S., 2002, Phys. Rev. D, 66, 103511
Lewis A., Challinor A., Lasenby A., 2000, ApJ, 538, 473
Linder E. V., 2005, Phys. Rev. D, 72, 043529
Linder E. V., Cahn R. N., 2007, Astropart. Phys., 28, 481
Macaulay E., Wehus I. K., Eriksen H. K., 2013, Phys. Rev. Lett., 111, 161301
Planck Collaboration XIII, 2016, A&A, 594, A13
Planck Collaboration XIV, 2016, A&A, 594, A14
Pogosian L., Silvestri A., 2016, Phys. Rev. D, 94, 104014
Pogosian L., Silvestri A., Koyama K., Zhao G.-B., 2010, Phys. Rev. D, 81, 104023
Reid B. et al., 2016, MNRAS, 455, 1553
Riess A. G. et al., 2011, ApJ, 730, 119
Riess A. G. et al., 2016, ApJ, 826, 56
Ross A. J. et al., 2016, MNRAS, 464, 1168
Sachs R. K., Wolfe A. M., 1967, ApJ, 147, 73
Samushia L., Percival W. J., Raccanelli A., 2012, MNRAS, 420, 2102
Sánchez A. G. et al., 2017a, MNRAS, 464, 1493
Sánchez A. G. et al., 2017b, MNRAS, 464, 1640
Satpathy S. et al., 2017, MNRAS, 469, 1369
Sievers J. L. et al., 2013, J. Cosmol. Astropart. Phys., 1310, 060
Silvestri A., Pogosian L., Buniy R. V., 2013, Phys. Rev. D, 87, 104015
Simpson F. et al., 2013, MNRAS, 429, 2249
Smee S. et al., 2013, AJ, 146, 32
Sollerman J. et al., 2009, ApJ, 703, 1374
Song Y.-S., Percival W. J., 2009, J. Cosmol. Astropart. Phys., 0910, 004
Song Y.-S., Zhao G.-B., Bacon D., Koyama K., Nichol R. C., Pogosian L., 2011, Phys. Rev. D, 84, 083523
Song Y.-S. et al., 2015, Phys. Rev. D, 92, 043522
Story K. T. et al., 2013, ApJ, 779, 86
Sullivan M. et al., 2011, ApJ, 737, 102
Weinberg D. H., Mortonson M. J., Eisenstein D. J., Hirata C., Riess A. G., Rozo E., 2013, Phys. Rep., 530, 87
Zhao G.-B., Pogosian L., Silvestri A., Zylberberg J., 2009, Phys. Rev. D, 79, 083513
Zhao G.-B., Li H., Linder E. V., Koyama K., Bacon D. J., Zhang X., 2012, Phys. Rev. D, 85, 123546

This paper has been typeset from a TEX/LATEX file prepared by the author.